Biosensors and Bioelectronics 141 (2019) 111408

Contents lists available at ScienceDirect

Biosensors and Bioelectronics

journal homepage: www.elsevier.com/locate/bios

'Electrical viscosity' of piezoresistive sensors: Novel signal processing method, assessment of manufacturing quality, and proposal of an industrial standard

Franz Konstantin Fuss*, Adin Ming Tan, Yehuda Weizman

Smart Equipment Engineering and Wearable Technologies Program, Centre for Design Innovation, Swinburne University of Technology, Melbourne, Australia

ARTICLE INFO

Keywords:
Piezoresistive sensor
Electrical viscosity
Fractional calculus
Hysteresis
Drift
Manufacturing quality.

ABSTRACT

Piezoresistive sensors become increasingly important in wearable devices, specifically sensors printed with piezoresistive inks. The electrical viscosity of these sensors causes phenomena such as stress relaxation, creep and hysteresis. This compromises sensor calibration and leads to inaccurate results. When subjecting a sensor to loading and unloading, the subsequent calculation of the fractional time derivative of the conductance leads to the elimination of the hysteresis. The order of the fractional derivative equals the magnitude of the sensor's viscosity. In our study, the viscosity of several pressure sensors was determined with a material testing machine and ranged from 0.55% to 22.35%. We found that shunt-mode sensors are less viscous than through-mode sensors. In addition, if a viscous material is placed on top of the sensor, then its viscosity increases. This is important as some calibration devices for pressure sensor arrays use rubber bladders which are viscous. From the perspective of manufacturing, the variation of the viscosity across a sensor array accounts for the quality of the pressure sensor mat and should be kept to a minimum. An industry standard is proposed that calculates and reports the sensor viscosity based on loading and unloading of the sensor and calculating the fractional time derivative of the conductance, whose fractional order reduces the pressure - conductance hysteresis to zero and thereby corresponds to the sensor's viscosity.

1. Introduction

Piezoresistive sensors, e.g. pressure sensors, become increasingly important in wearable devices, specifically in sensor arrays for pressure mapping printed with piezoresistive inks. The pressure applied to such sensors is a function of their electrical conductivity. Yet, 'the' conductivity is a relative and simplified term, as loading (positive force rate) and unloading (negative force rate) exhibit differences in electrical conductivity, such that the loading conductivity is smaller (!) than the unloading one at the same pressure level. This conductivity hysteresis is caused by the viscosity of the sensor, resulting in a spectrum of well-known time-dependent effects, such as stress relaxation, creep (often incorrectly and mistakenly denoted as 'drift'; used e.g. by Pamar et al., 2017), velocity dependency, overshoot after ramp loading, stress transfer, cyclic loading transient phase, and hysteresis. The more pronounced the viscous effects are, the smaller is the sensor's accuracy, mainly because of the discrepancy between loading and unloading, and delayed effects such as the decrease in electrical conductivity lagging behind the reduction of force or pressure. The classical example is the creep effect, where a static (and therefore constant) load leads to an asymptotically increasing electrical conductivity, which would usually be interpreted (from the calibration function) as an increasing load. Equally, if a sensor is statically calibrated at an apparent, but non-existing, steady-state of the creep effect, then the pressure is underestimated in dynamic situations when using the calibration function obtained.

There is literature available on certain aspects of 'electrical viscosity' phenomena and models; however, no consensus has been reached so far. In their review of '*Recent developments in bio-monitoring via … wearable strain sensors*', Lu et al. (2019) exemplify the sensor hysteresis from a figure of Gong et al. (2015), and mention that '*resistive-type strain sensors typically suffer large hysteresis*' (Gong et al., 2015). However, the authors did not suggest any method for quantification of the viscous effect of piezoresistive sensors. The models that have been used so far for modelling the viscous effect of piezoresistive sensors can be classified as linear and non-linear, and are comparable to the models used for modelling visco-eleastic solids.

Kalantari et al. (2012) modelled the viscosity of piezoresitive force

* Corresponding author.
E-mail address: fkfuss@swin.edu.au (F.K. Fuss).

https://doi.org/10.1016/j.bios.2019.111408
Received 6 May 2019; Accepted 2 June 2019
Available online 05 June 2019

sensors as a Standard Linear Solid (Zener model, spring and Voigt model [i.e. spring and dashpot in parallel] in series). Giovanelli and Farella (2016) applied the same model for the purpose of correcting errors produced by the sensor's creep. Ding et al. (2007) used the Burgers model (i.e. spring, Voigt model and dashpot in series) for modelling the change of electrical resistance of piezoresistive sensors. Wang et al. (2011) suggested a generalised Voigt model (several Voigt models in series plus one series spring) for modelling purposes. Lacasse et al. (2010) applied the same model to the unloading part of a rectangular pressure step for correction of the signal. They called their model an 'augmented Burgers model' plus one additional spring in parallel with the series dashpot, resulting in two series Voigt models and a series spring. Kost et al. (1994) applied a quasi-linear visco-elastic model in the form of a generalised Kelvin 3-element model (spring and Maxwell model [spring and dashpot in series] in parallel) with non-linear springs. Wang et al. (2009) modelled the resistance relaxation with a Wiechert model (several Maxwell models in parallel plus one parallel spring).

Non-linear models were used by Voet et al. (1971), Sircar et al. (1971), and Zheng et al., (2004) namely power law models for determining the creep and relaxation rates. Weizman and Fuss (2015) and Weizman (2016) investigated the creep of conductance of piezoresistive sensors with power- and log-law models and concluded that the creep follows a power-law better than a log law does, even if the mechanical stress relaxation of the polymer sensor was clearly characterised by a log-law model. The studies quantified the viscosity of the sensors from the power exponent of time, in the same way as Voet et al. (1971) and Sircar et al. (1971) did.

There are model-independent methods for hysteresis compensation of sensors unrelated to specific viscosity modelling. For example, Hall et al. (2008) compensated the hysteresis of force sensing resistors with 4th order polynomial regression models. Oppermann et al. (2010) applied the inverse Preisach (1935) hysteresis model for compensating the hysteresis caused by the magneto-elastic effect of magnetic force sensors.

It seems that there is no consensus on which model to use for characterising the viscous behaviour of piezoresistive materials. Yet, the nonlinear power-law model is advantageous over the log-law model and linear models, as the loss tangent (the ratio of loss modulus to storage modulus) is only dependent on the viscosity constant, not influenced by any other parameter. In log-law and linear models, the loss tangent is influenced by viscosity coefficients, stiffness of springs, and frequency of cyclic loading (Fuss, 2015a).

Companies selling piezoresistive inks for printing of pressure sensors provide calibration curves consisting only of a few data points (e.g. pressure vs. resistance), without reporting the degree of hysteresis, let alone the magnitude of the viscosity itself. The latter could be directly derived from loading the sensor and determining the creep rate, i.e. the power exponent of the electrical conductivity increasing with time. This method is, however, not time-efficient as the creep rate is measured over very large times. The reason for this is that a sensor cannot be loaded instantaneously, but only gradually, i.e. by a steep ramp function of the load. If loaded by a ramp function, the signal overshoots and approaches the data expected from instantaneous loading (Heaviside function of the load) asymptotically only at larger times. This principle was demonstrated mathematically (Fuss, 2012) and proven experimentally (Weizman, 2016) in piezoresitive materials. If creep is measured at shorter times, the viscosity constant will be overestimated. When pressure sensor arrays are tested (and calibrated) at an industrial scale, time is critical.

An industrial standard for reporting the electro-mechanical properties of piezoresistive sensors is therefore overdue, considering their importance in the booming wearable tech industry. If a sensor's viscosity parameter, pressure range and sample calibration curves (including hysteresis) are reported properly, together with applying standardised test methods and reporting repeatability and reliability, then the customers would have accurate data for selecting the most accurate and best performing sensor at their disposal. The accuracy of a wearable device is only as good as the incorporated sensors are. Furthermore, companies, manufacturing printed pressure sensors from piezoresitive inks, are not only able to advise their customers of the best performing inks, but would also be able to assess and control the quality of their printed sensors, e.g. in terms of consistency of electro-mechanical properties.

Based on the aforementioned issues, the aim of this paper is to provide the theoretical background of 'electrical viscosity' and to suggest a simple and fast signal processing method for determining the viscosity constant of piezoresistive sensors. This method can be used for correcting viscous signals (within reason), but would serve even more so for establishing an industry standard for reporting sensors' viscosity as well as for assessment of the manufacturing quality of piezoresistive sensors. The specific aims of this paper are to:

- use the power model of viscoelastic solids for mathematical modelling of the 'electrical' viscosity;
- develop a theoretical analysis of signals of viscous and inviscid sensors by using fractional calculus;
- use experimental observation for understanding the behavior of various viscous piezoresistive sensors;
- apply numerical simulation to convert the experimentally obtained signal of a viscous sensor to the one of a theoretical inviscid sensor, for quantifying the amount of 'electrical' viscosity; and
- propose a new industry standard for easily determining the exact viscosity value of a piezoresistive sensor, providing the customer with critical information.

2. Method

2.1. Objectives

Piezoresistive sensors are affected by viscous effects, resulting in hysteresis in the pressure-conductance curve. Consequently, precise calibration of the sensor is impossible, or at least affected by severe inaccuracies.

For assessing the electrical viscosity of a piezoresistive sensor, a non-linear visco-elastic power-law model was selected, as its viscosity is not affected by other material properties (modulus), experimental conditions (frequency of loading cycles) and does not change with time (Fuss, 2015a). It is therefore a single parameter that can be easily reported for quantifying the viscosity of a sensor. Other models, such as linear models (standard linear solid and other models consisting of elastic springs and viscous dampers), and non-linear visco-elastic log-law models, suffer from the aforementioned problems (Fuss, 2015a).

The non-linear visco-elastic power-law model is inherently linked to fractional calculus, as seen from the non-integer exponent of '*s*', the complex variable of transformed functions. Fractional calculus extends beyond ordinary calculus, such as derivatives and integrals of integer orders, to non-integer orders. For example, there are half-derivatives, which are half-way between the original function and its first derivative. Semi-differentiating a function twice results in its first derivative. A classical example of a semi-integral solution is the tautochrone problem (Abel, 1823), where the main finding is "*a curve … such that the time required for a particle to slide down the curve to its lowest point is independent of its initial placement on the curve*" (Oldham and Spanier, 1974).

In addition to solving theoretical problems, fractional calculus finds a multitude of applications in the fields of visco-elasticity, diffusion, attenuation, dispersion, thermoelasticity, image processing, epidemiological models, biological tissue modelling, solute transport, hydrological cycles, chemical reactions, and economic processes (Sun et al., 2018). With the present research, 'electrical viscosity' is a new addition to the list.

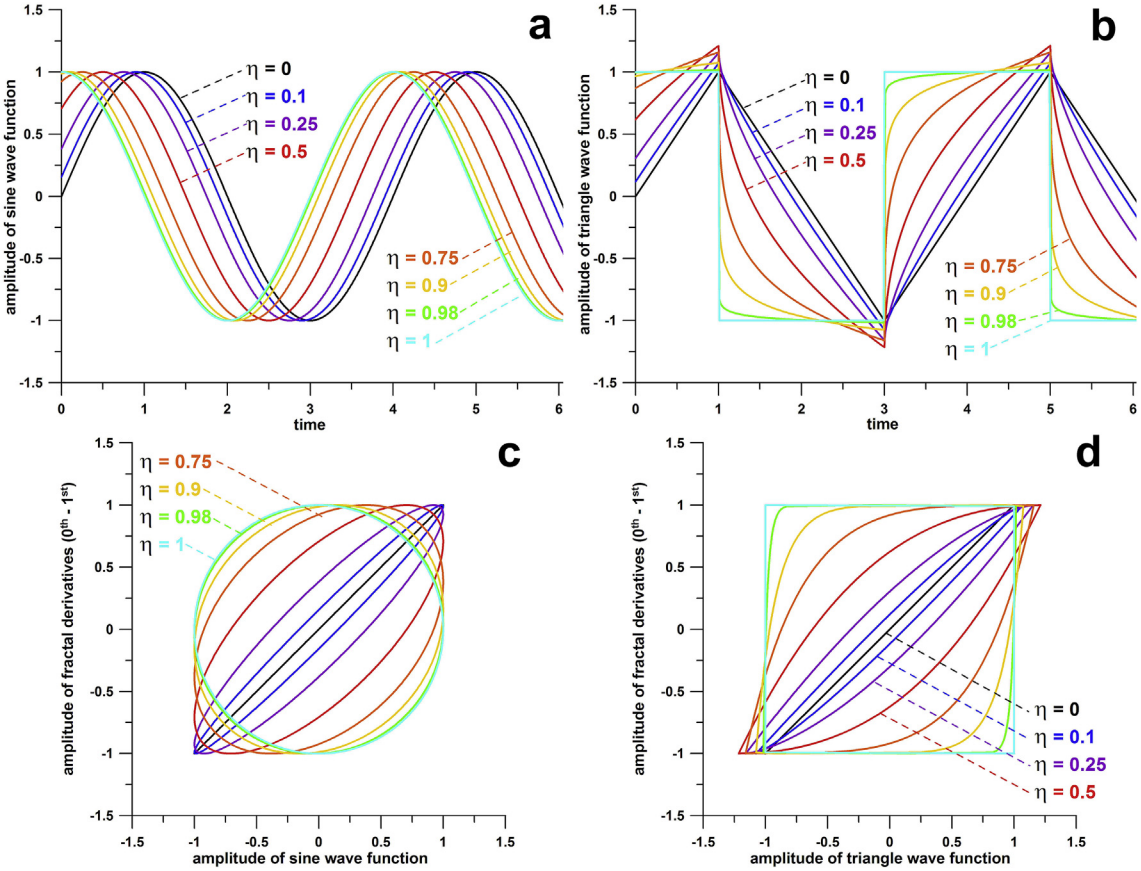

Fig. 1. a, **b**: amplitude of sine (**a**) and triangular (**b**) wave functions against time (arbitrary unit), for fractional derivatives of orders: 0 (original functions), 0.1, 0.25 (quarter derivative), 0.5 (semiderivative), 0.75 (three quarter derivative), 0.9, 0.98 and 1 (first derivative); note that in the sine function, fractional derivatives are characterised by a phase shift without changing the shape of the functions, whereas in triangular functions, a phase shift is missing and the function changes its shape from ramp functions to step functions; **c**, **d**: amplitude of fractional derivatives against their original sine (**c**) and triangular (**d**) functions; the amplitude of fractional derivatives corresponds to the pressure measured with piezoresistive sensors.

The method section starts with a brief explanation and discussion of power-law viscoelasticity of solids and their relationship to fractional calculus. For example, it is shown that the stress in a viscoelastic solid is a fractional derivative of the strain.

These principles are then applied to piezoresistive sensors in the sense that the electrical conductance of the sensor, changing with varying pressure, is a fractional integral of the pressure. As such, when subjecting the measured viscous conductance of a sensor to fractional derivation with time, the fractional order of the derivative at the point when the hysteresis vanishes equals the degree of viscosity of that sensor, and the measured viscous conductance is converted to a hypothetical inviscid conductance.

Subsequently, piece-wise fractional differentiation equations are provided for calculating the fractional derivatives of conductance signals.

Based on these principles, the concepts of actual and virtual signals are introduced to exemplify the method of extracting the viscosity with fractional calculus.

Finally, the experimental methods are described, and the pressure sensors tabulated in terms of viscosity. These sensors include screen printed insoles used for measuring the pressure at the foot soles.

2.2. Mathematical principles and concepts

For modelling the electrical viscosity of a piezoresistive sensor, the principles of visco-elastic solids have to be reviewed for reference purposes.

The constitutive equation of a power-law visco-elastic material derived from stress relaxation $\sigma = E\varepsilon_0\, t^{-\eta}$ is

$$\hat{\sigma} = s^{\eta}\hat{\varepsilon}\; E\; \Gamma(1-\eta) \tag{1}$$

(Fuss, 2012, 2015a), where $\hat{\varepsilon}$ and $\hat{\sigma}$ denote the Laplace-transformed strain and stress, respectively, E is the modulus, η is the viscosity, Γ denotes a gamma function, and s is the complex variable of transformed functions.

Eq. (1) reveals the intrinsic properties of the power law model:

a) $0 \le \eta < 1$, as the Gamma function in Eq. (1) approaches infinity when η approaches 1, and
b) the stress σ is the η^{th} (fractional) derivative of the strain ε, times the constant $E\Gamma(1-\eta)$ (Fuss, 2012).

If derived from creep, $\varepsilon = E^{-1}\sigma_0\, t^{\eta}$,

$$\hat{\sigma} = s^{\eta}\hat{\varepsilon}\; E\; \Gamma^{-1}(1+\eta) \tag{2}$$

where the difference between Eq. (1) and Eq. (2) is merely the multiplier in the form of a Gamma function. These multipliers are subsequently reduced to the constant C, which equals to $\Gamma(1-\eta)$ if the constitutive equation is derived from stress relaxation, or to $\Gamma^{-1}(1+\eta)$ if derived from creep. The constitutive equation and its inverse transforms are

$$\hat{\sigma} = s^{\eta}\hat{\varepsilon}\; E\; C \rightarrow \sigma = E\; C\; \frac{\mathrm{d}^{\eta}}{\mathrm{d}t^{\eta}}\varepsilon \tag{3}$$

where the stress σ is the 0^{th}, half or 1st derivative of the strain ε if η is 0, 0.5 or 1, respectively.

Alternatively, Eq. (3) can be expressed in terms of force F, deflection x, and stiffness k

$$\hat{F} = s^{\eta}\hat{x}\ k\ C \rightarrow F = k\ C\ \frac{\mathrm{d}^{\eta}}{\mathrm{d}t^{\eta}}x \tag{4}$$

The viscosity constant η is usually obtained from cyclic testing, by subjecting the material to sinusoidal strain ε or deflection x

$$x = x_0 \sin(2\pi f\ t) \tag{5}$$

where x_0 denotes the magnitude of the deflection, and f denotes the frequency of the testing cycles, resulting in the force being the η^{th} (fractional) derivative (Fig. 1a) of the deflection function

$$F = x_0 kC\ \frac{\mathrm{d}^{\eta}}{\mathrm{d}t^{\eta}} \sin(2\pi f\ t) = x_0 kC\ (2\pi f)^{\eta} \sin\left(2\pi f\ t + \eta\frac{\pi}{2}\right) \tag{6}$$

(Fuss, 2015a) where $\eta\pi/2$ is the phase shift δ, and $\tan\delta = \tan(\eta\pi/2)$ equals the loss tangent.

Note that Eq. (6) represents the steady state of the force function if the lower limit of the inverse operation of the Riemann-Liouville fractional integration is $-\infty$, which equals the inverse operation of the Weyl integral (Weyl, 1917).

The problems related to deriving the viscosity constant η from cyclic testing are that standard material testing machines (e.g. Instron) cannot generate sinusoidal loading functions, but do provide the more common triangular functions (ramp up and down) instead (Fig. 1b). Thus, η cannot be extracted from a phase shift, which in fact does not exist in fractional derivatives of a triangle wave function (Fig. 1b). However, the hysteresis is apparent in both sine and triangle wave functions (Fig. 1c and d). In the former, the hysteresis is generated by the phase shift; whereas the shape of the sine wave remains unaffected by fractional derivation (Fig. 1c). In the latter, the linear segments of the triangle wave function become non-linear by fractional derivation, thus transforming the shape change to a hysteresis (Fig. 1d).

From Eq. (3) and Eq. (4), the stress σ or force F are fractional derivatives of the strain ε or displacement x. ε or x are applied to the test sample by the material testing machine and are therefore the primary input or data. σ or F are secondary or output data and depend on the viscosity. In a more viscous material, the force peak is smaller when subjected to a triangular displacement function when compared to a less viscous material, even when they have the same stiffness. σ or F are derived from the measured ε or x by means of a calibration function. For establishing the calibration function, ε or x is applied to the material as functions of time, according to Eq. (5). The reaction force or stress of the material subjected to displacement or strain is therefore a fractional (η^{th}) derivative of the time function of x or ε, according to Eq. (3) and Eq. (4).

These *mechanical* principles are applied to the *electrical* signal of piezoresistive sensors. The 'electrical viscosity' is defined as hysteretic behaviour of the sensor's calibration function. In electrical terms, the pressure p is derived from the measured electrical conductance G of the sensor. When experimentally loading and unloading the sensor and plotting p against G, the hysteretic behaviour of the calibration function becomes evident. Compared to the mechanical quantities, p corresponds to F or σ, and G corresponds to x or ε. In contrast to mechanical quantities, p is the input and therefore the primary data, as the pressure is applied to the piezoresistive sensor; and G is the measured output and therefore the secondary data. It is evident that the conductance G cannot be applied to a piezoresistive sensor in order to produce pressure.

Eq. (3) is re-written in electrical terms:

$$\hat{p} = s^{\eta}\hat{G}\ m\ C \tag{7}$$

where m is a multiplier, representing the calibration factor; note that m is usually not a constant and therefore linked to the (non-linear) calibration function.

Inverting and inverse-transforming Eq. (7)

$$\hat{G}_{\eta>0} = s^{-\eta}\frac{\hat{p}}{m}\frac{1}{C} \rightarrow G_{\eta>0} = \frac{1}{C}\frac{d^{-\eta}}{dt^{-\eta}}\left(\frac{p}{m}\right) \tag{8}$$

shows that the measured viscous conductance $G_{\eta>0}$ is a fractional integral of the pressure. Note that the subscript '$\eta > 0$' means $0 < \eta < 1$. If $\eta = 0$, then Eq. (8) reduces to

$$\hat{G}_{\eta=0} = \frac{\hat{p}}{m}\frac{1}{C} \rightarrow G_{\eta=0} = \frac{p}{m} \tag{9}$$

By substitution

$$G_{\eta>0} = \frac{1}{C}\frac{d^{-\eta}}{dt^{-\eta}}(G_{\eta=0}) \rightarrow G_{\eta=0} = C\frac{d^{\eta}}{dt^{\eta}}(G_{\eta>0}) \tag{10}$$

Eq. (10) explains the principle that the theoretical inviscid conductance, $G_{\eta=0}$, is a fractional derivative of the measured viscous conductance $G_{\eta>0}$. Therefore, by calculating the η^{th} derivative of $G_{\eta>0}$, the viscous property of G is converted to an inviscid state. The actual value of the pressure p remains thereby unchanged. Ultimately, when plotting p against $G_{\eta>0}$, the hysteresis vanishes. As such, the exact value of η is determined by finding the order of the fractional derivative of $G_{\eta>0}$ at the moment the hysteresis vanishes.

The fractional derivative is calculated piece-wise from finite segments of conductance - time data. The order of the fractional derivative, i.e. the viscosity constant η, is determined numerically, by equating the area under the calibration curve with 0.

Note that piezoresistive sensors are not modelled as visco-***elastic*** solids in this paper, even if the constitutive equations of visco-elastic solids are used. The reason for this is that the elastic component, namely E, the modulus ($\mathrm{d}\sigma/\mathrm{d}\varepsilon$), is a mechanical property. The electrical counterpart would be the gauge factor, $(\Delta R/R)/\varepsilon$ [where R denotes the electrical resistance], of strain gauges, or the sensitivity of a piezoresistive sensor ($\mathrm{d}G/\mathrm{d}F$, $\mathrm{d}G/\mathrm{d}p$, $\mathrm{d}G/\mathrm{d}\sigma$). Even if the loss tangent ($\tan\delta$), representing the phase shift δ and therefore the viscosity, is defined as the ratio of loss modulus (energy dissipation inside the material due to viscous friction) to storage modulus (stored energy, when released, accounting for the elastic response of a material), the loss tangent of a power model is related to the viscous property but not to the elastic property whatsoever, since $\tan\delta = \tan(\eta\pi/2)$, according to Eq. (6). Piezoresistive sensors are therefore modelled as electrically ***viscous*** structures in this paper. The electrical analogue to the elastic property, however, i.e. the sensitivity, is still considered when plotting the load (force F, pressure p, stress σ) against the conductance G. (cf. Fig. 3b).

2.3. Piece-wise fractional differentiation

If the conductance G is measured across two time stamps, and G within this time window is approximated linearly as

$$G_{\eta>0} = kt \tag{11}$$

then the hypothetical (i.e. inviscid) conductance $G_{\eta=0}$ is

$$G_{\eta=0} = \frac{\mathrm{d}^{\eta}}{\mathrm{d}t^{\eta}}G_{\eta>0} = k\frac{\Gamma 2}{\Gamma(2-\eta)}t^{1-\eta} = k\frac{1}{\Gamma(2-\eta)}t^{1-\eta} = k\frac{t^{1-\eta}}{\Gamma(2-\eta)} \tag{12}$$

applicable if the ramp starts at $t = 0$ and continues till $t = \infty$. Subsequently, the multiplier $\Gamma^{-1}(2-\eta)$ will be removed from the following equations, as a common multiplier does not change the principle, nor has any effect on the viscosity, η. However, removing the multiplier $\Gamma^{-1}(2-\eta)$ has an effect on the magnitude of hypothetical (i.e. inviscid) conductance $G_{\eta=0}$. The reason for calculating $G_{\eta=0}$ by means of a fractional derivative of $G_{\eta>0}$ is to collapse the hysteresis. Irrespective of the magnitude of $G_{\eta=0}$, the hysteresis vanishes at the η^{th} derivative of $G_{\eta>0}$, since scaling of the amplitude does not affect the viscosity, η. Further justification for removal of the Gamma term is provided at the end of section 'D' (Concept of virtual signal) below.

If the time segment (ramp function of $G_{\eta>0}$) starts at $t = 0$ and ends

at T_1, then

$$G_{\eta=0} = kt^{1-\eta} - k(t - T_1)^{1-\eta} \tag{13}$$

where the first argument represents the initial ramp and the 2nd one the time-shifted ramp mirrored about the zero line (hence the negative sign of the 2nd term), such that sum of both arguments represents the infinite dwell after the initial ramp. As the term $(t - T_1)$ is negative if $t < T_1$, Eq. (13) returns imaginary results. Therefore, it is multiplied by the Heaviside function H of $t - T_1$, which sets negative data to 0:

$$G_{\eta=0} = kt^{1-\eta} - k\{[H(t - T_1)](t - T_1)\}^{1-\eta} \tag{14}$$

If the time segment (ramp) starts at T_1 and ends at T_2, then

$$G_{\eta=0} = k\{[H(t - T_1)](t - T_1)\}^{1-\eta} - k\{[H(t - T_2)](t - T_2)\}^{1-\eta} \tag{15}$$

For two consecutive time segments:

$$\begin{aligned} G_{\eta=0} = {} & k_1 t^{1-\eta} - k_1\{[H(t - T_1)](t - T_1)\}^{1-\eta} + k_2 \\ & \{[H(t - T_1)](t - T_1)\}^{1-\eta} - k_2\{[H(t - T_2)](t - T_2)\}^{1-\eta} = \\ & k_1 t^{1-\eta} + (k_2 - k_1)\{[H(t - T_1)](t - T_1)\}^{1-\eta} - k_2\{[H(t - T_2)](t - T_2)\}^{1-\eta} \end{aligned} \tag{16}$$

For n consecutive time segments:

$$\begin{aligned} G_{\eta=0} = {} & k_1 t^{1-\eta} + \left(\sum_{i=1}^{n-1} (k_{i+1} - k_i)\{[H(t - T_i)](t - T_i)\}^{1-\eta}\right) \\ & - k_n\{[H(t - T_n)](t - T_n)\}^{1-\eta} \end{aligned} \tag{17}$$

Note that the loading/unloading function does not necessarily have to be a triangular wave, and that the piece-wise fractional derivation can be applied to any loading/unloading functions, which evidently includes sine waves.

2.4. Concept of virtual signal

If a piezoresistive sensor is loaded and unloaded with a triangular loading pattern, and the pressure exerted on sensor is plotted against the conductance G of sensor then the hysteresis behaviour becomes apparent. The area under curve is therefore larger than zero, as the pressure of the loading segment is higher than the one of the unloading one, at the same conductance G.

Subsequently, the G-signal is corrected such that the area under curve becomes zero. As the G-signal measured is the fractional (η^{th}) integral of a hypothetical (virtual) inviscid signal, the correction method of G is simply the calculation of the fractional (η^{th}) derivative of the measured conductance G. The viscosity of the sensor corresponds to η determined through the correction process.

If the loading events of the triangular loading pattern are separated by zero load segments, then these segments can result in negative data after fractional differentiation. As the inviscid conductance $G_{\eta=0}$ cannot be negative, the negative data are set to zero.

To put this into context, different virtual and actual signals have to be considered (Fig. 2):

Let y be the virtual inviscid signal, i.e. G of an inviscid sensor as a function of time. As an inviscid signal y is an ideal one, but non-existent as long as the actual viscous signal exhibits hysteretic behaviour, it is denoted 'virtual'.

1) Virtual inviscid signal y (VIS):

$$VIS = y = \frac{\mathrm{d}^{\eta}}{\mathrm{d}t^{\eta}}\left(\frac{\mathrm{d}^{-\eta}}{\mathrm{d}t^{-\eta}}y\right) \tag{18}$$

where y is the fractional derivative of the fractional integral of y. The virtual inviscid signal is a conceptual and hypothetical one, the result of correction via the η^{th} derivative of the actual viscous signal. The virtual inviscid signal is an imperfect one, as it can exhibit negative values.

The virtual viscous signal is then:

2) Virtual viscous signal (VVS)

$$VVS = \frac{\mathrm{d}^{-\eta}}{\mathrm{d}t^{-\eta}}y \tag{19}$$

i.e. the fractional (η^{th}) integral of the virtual inviscid signal, Note the negative data in both virtual signals (Fig. 2). Removing the negative data of the virtual viscous signal (with a Heaviside function) yields the actual viscous signal measured by the piezoresistive sensor:

3) Actual viscous signal (AVS)

$$AVS = \frac{\mathrm{d}^{-\eta}}{\mathrm{d}t^{-\eta}}y\ \mathrm{H}\left(\frac{\mathrm{d}^{-\eta}}{\mathrm{d}t^{-\eta}}y\right) \tag{20}$$

which is the product of the virtual viscous signal and the result of its Heaviside function. This measured sensor signal is corrected in order to quantify the viscosity of the sensor, thereby resulting in the imperfect virtual inviscid signal with negative data:

4) Imperfect virtual inviscid signal (IVIS)

$$IVIS = \frac{\mathrm{d}^{\eta}}{\mathrm{d}t^{\eta}}\left[\frac{\mathrm{d}^{-\eta}}{\mathrm{d}t^{-\eta}}y\ \mathrm{H}\left(\frac{\mathrm{d}^{-\eta}}{\mathrm{d}t^{-\eta}}y\right)\right] \tag{21}$$

which is the result of the correction method (η^{th} derivative of actual viscous signal). After removal of its negative data, we obtain the actual inviscid signal, resulting from the same sensor if its viscosity were zero:

5) Actual inviscid signal (AIS)

$$AIS = \frac{\mathrm{d}^{\eta}}{\mathrm{d}t^{\eta}}\left[\frac{\mathrm{d}^{-\eta}}{\mathrm{d}t^{-\eta}}y\ \mathrm{H}\left(\frac{\mathrm{d}^{-\eta}}{\mathrm{d}t^{-\eta}}y\right)\right]\mathrm{H}\left\{\frac{\mathrm{d}^{\eta}}{\mathrm{d}t^{\eta}}\left[\frac{\mathrm{d}^{-\eta}}{\mathrm{d}t^{-\eta}}y\ \mathrm{H}\left(\frac{\mathrm{d}^{-\eta}}{\mathrm{d}t^{-\eta}}y\right)\right]\right\} \tag{22}$$

which is the Heaviside function of the imperfect virtual inviscid signal, but also the virtual inviscid signal y multiplied by its Heaviside function: y H(y).

The effect of removing the gamma function term $\Gamma^{-1}(2–\eta)$ in Eq. (12), and subsequent equations, is that any common multiplier applied to, or removed from, Eq. (17) changes the amplitude of the AIS. This leads to the fact that the AIS represented as a graph of pressure p vs. inviscid conductance $G_{\eta=0}$ (cf. Fig. 3b) is compressed leftward or stretched rightward. The degree of viscosity is thereby not affected, as the hysteresis collapses entirely at the η^{th} derivative of $G_{\eta>0}$, irrespective of any (common) multiplier applied to or removed from $G_{\eta=0}$.

2.5. Experiments

We tested different piezoresistive sensors (Table 1), individual ones with Instron (5967, Instron Corporation, Massachusetts, USA) by using a triangular loading/unloading pattern (steady state). The printed sensor arrays were loaded with Trublu (Novel GmBH Inc, Munich, Germany) by using a non-linear, manually generated loading/unloading pattern after conditioning (steady state).

The calibration with Instron was performed by placing the sensors between two aluminium plates (40 x 40 mm, which served as electrodes for sensors 1-6, Table 1). For the single cell (sensors 11, 12; Table 1) of the in-house-developed insole (and printed by Central Midori International, Singapore), a wooden spacer and a silicone rubber one, cut to the size and shape of the sensor, were placed on the sensor.

The Trublu calibration device compressed the sensor between the bottom metal plate and a rubber sheet. The latter constituted one side of an air bladder. Loading of the sensors was achieved by increasing the pressure continuously up to 0.6 MPa, followed by initial pronounced unloading down to 0.5 MPa and subsequent unloading with a flatter gradient. The pressure was indicated by an analog manometer and recorded as a digital file.

The sensor was placed in series with a reference resistor and the voltage drop was measured across the reference resistor equivalent to a

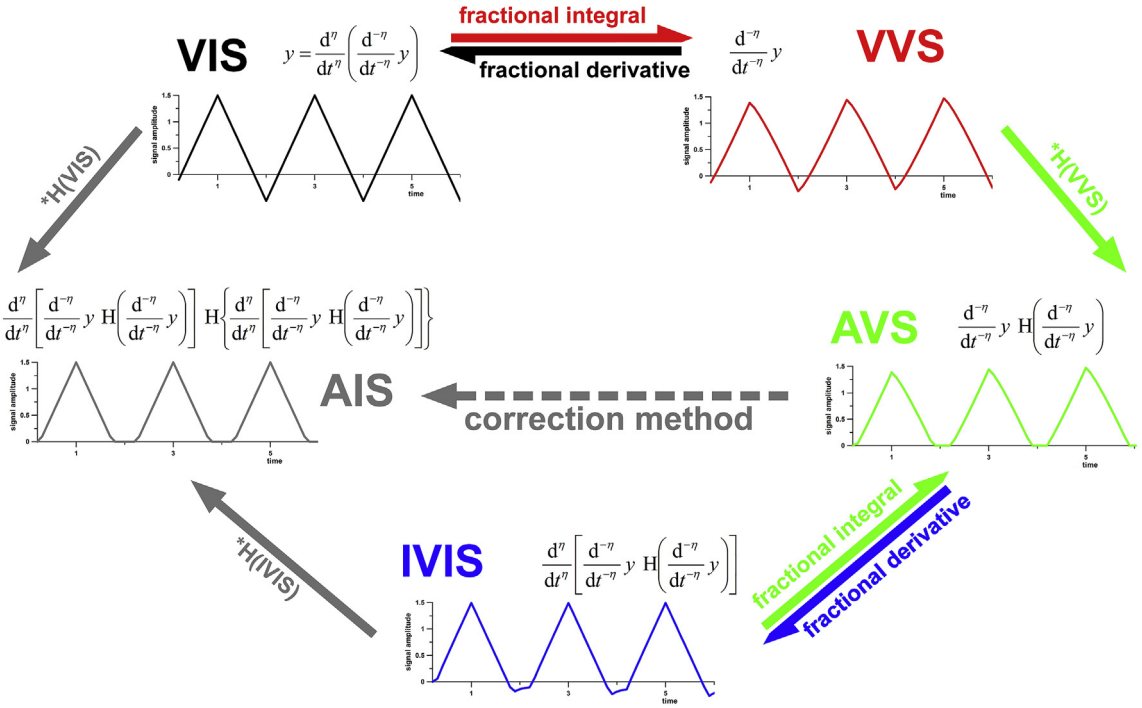

Fig. 2. Concept of virtual and actual signals and flowchart of the signal correction method. VIS = virtual inviscid signal; VVS = virtual viscid; AVS = actual viscid (measured); IVIS = imperfect virtual inviscid; AIS = actual inviscid (corrected signal); '*H(VIS)' means that the VIS is multiplied by its Heaviside function; the dashed arrow denotes the correction method (which has to take a detour via the IVIS). The hysteretic signal before correction is seen when plotting pressure vs. AVS (measured; cf. Fig. 3b); after correction, the signal becomes inviscid and thus inhysteretic when plotting pressure vs AIS (fractional derivative of AVS and removal of negative values of IVIS; cf. Fig. 3b). Arrows labelled with '*H' are unidirectional, as reverting actual signals (without negative values) back to virtual ones (with negative values) is impossible, e.g. it is impossible to revert AIS, i.e. $y^*H(y)$, back to VIS, i.e. y, because $y^*H(y)/H(y) \neq y$, as negative y of virtual signals correspond to zero y of actual signals after applying the Heaviside function; accordingly, $H(y)/H(y) = 0/0$, resulting in un-defined values.

voltage divider. The magnitude of the reference resistor was selected to match the resistance of the sensor at maximum load to achieve best resolution.

For processing, the peak data of force or pressure and the ones of conductance were aligned; and force or pressure was plotted against conductance for assessment of hysteresis. Subsequently, a Matlab routine (R2017a, MathWorks, Inc., Natick, Massachusetts, United States) was written, based on Eq. (17), to determine the viscosity of the sensor signal with respect to the applied force or pressure.

The viscosity data of the three layers of the 2nd printed sensor array (sensor structure 15; Table 1) were compared with the Kruskal-Wallis test (as one layer was not normally distributed according to the Shapiro-Wilk test); and individual layers with 2 post-hoc tests, Conover and Dunn test, both adjusted by the Holm FWER method and Benjamini-Hochberg FDR method. Significant differences were established if $p < 0.05$.

3. Results

Fig. 3 shows a typical example of force vs. conductance (including the hysteresis), as well as both against time, uncorrected and corrected, of sensor 12 (cf. Table 1). The resulting viscosity constant (100η) of this test was 11.03%. Even if 11% seems to be small, the hysteresis is considerably large, with a maximum force F differential of

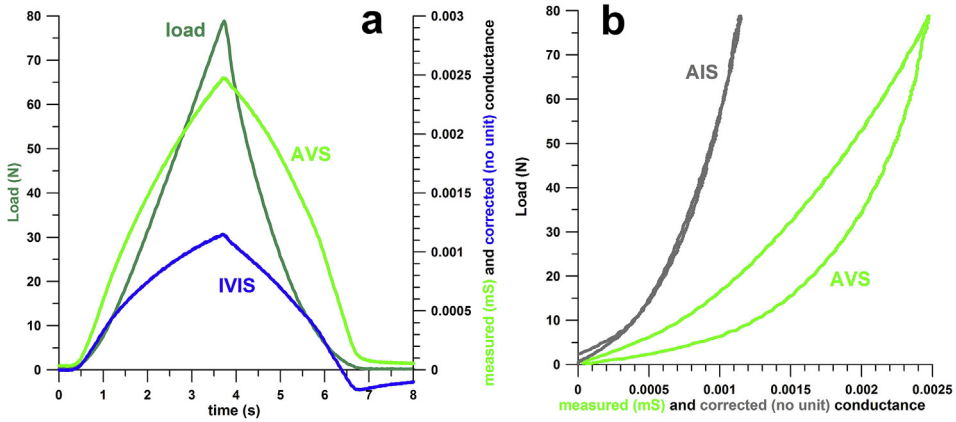

Fig. 3. a: load (N) and conductances (AVS = measured actual viscous signal [mS; cf. Fig. 2]; and IVIS = corrected but imperfect virtual inviscid signal [no unit; cf. Fig. 2]) against time; the corrected conductance is the 0.1103rd time derivative of the measured conductance, as the sensor's viscosity is 11.03%; note that 1) the sensor was loaded with a silicone spacer which contributes to the relatively high viscosity; 2) that the corrected conductance as a fractional derivative of the measured conductance is unitless, as the unit of the original conductance (AVS) is Siemens, and the one of its 1st time derivative would be Siemens per second (this is also why removing $\Gamma^{-1}(2-\eta)$ from the equations does not have any effect; cf. text); 3) the conductance of the corrected signal (IVIS) is negative at the end of the unloading segment; **b**: load against conductances (AIS = corrected and actual inviscid signal [no unit; cf. Fig. 2]); note that 1) the corrected signal is the AIS (and no longer the IVIS) as the negative values were removed; 2) the conductance can never be exactly zero, because of the resistance in the unloaded state of the sensor being smaller than infinity; 3) the areas under the loading and unloading segments of the corrected conductance (AIS) are identical so that the hysteresis has vanished mathematically, even if the loading and unloading segments are not perfectly identical.

Table 1
Piezoresistive materials and their viscosity data (in %).

The viscosity is expressed as a percentage, as $0 \leq \eta < 1$; the viscosity shown in this table is therefore equal to 100η; sensors 13, 14 and 15 were tested only once (calibration with Trublu, Novel GmBH Inc, Munich, Germany); all other sensors were tested with Instron (5967, Instron Corporation, Massachusetts, USA) five times (5 samples of sensors 1-10, and one sample of sensor 11, 12, 13 [i.e. same physical sensor but 3 different spacers]); sensors 1-6 had a square shape with a side length of 40 mm; the in-house-developed smart insole (sensors 11-15) was printed by Central Midori International, Singapore.

Piezoresistive sensor structures	sensor structure number	average viscosity (%)	viscosity standard deviation (%)
Vinyl (electrostatic mat 1)	1	1.59	1.14
Electrostatic mat 2	2	1.81	1.78
Hard electrostatic foam	3	13.10	3.29
Soft electrostatic foam	4	16.51	4.06
Velostat, two layers (0.1 mm)	5	1.24	1.44
Thick Velostat, one layer (0.2 mm)	6	22.35	4.52
Sensitronics shunt mode 0.5" (printed)	7	0.55	0.85
Sensitronics shunt mode 1" (printed)	8	2.55	1.40
Sensitronics thru mode 1" (printed)	9	1.00	0.33
Taiwanese [Uneo Inc.] thru mode 1" (printed)	10	3.15	0.41
Printed smart insole, thru mode (centre front sensor; cf. Fig. 4) + wooden spacer	11	4.77	0.64
Printed smart insole, thru mode (centre front sensor) + silicone rubber spacer	12	11.03	0.09
Printed smart insole, thru mode (centre front sensor) + rubber mat (calibrated with Trublu)	13	16.92	—
Printed smart insole, thru mode (average of all 88 sensors) + rubber mat (calibrated with Trublu)	14	14.69	0.69
Printed smart insole, shunt mode (average of all 87 sensors) + rubber mat (calibrated with Trublu)	15	7.28	2.94

$\Delta_{max}F = 18.9$ N at a conductance of 1.86 µS (40.4% of the force on the loading curve; Fig. 3b).

Table 1 lists the viscosity results of different piezoresistive materials tests, including the test method. The highest average sensor viscosity measured was 22.35% (sensor 6; Table 1). The highest average individual sensor viscosity measured within a sensor array was 16.92% (sensor 13; Table 1). This specific viscosity was highly dependent on the material used for compressing this individual sensor (sensor 11/12/13): $100\eta = 16.92\%$ if calibrated with Trublu and compressed by its rubber bladder (sensor 13); $100\eta = 11.03\%$ if compressed by a silicone rubber spacer (sensor 12); and $100\eta = 4.77\%$ if compressed by a wooden spacer (sensor 11; Table 1).

In general, sensors 1-10 exhibited high standard deviations, which results from inconsistencies of the manufacturing process (be it the fabrication of sheet materials such as electrostatic mats and foams [sensors 1-6]; or the printing process of force resistive sensors [sensors 7-10]). Moreover, even the sensors within a 2D sensor array were not consistently printed. In two different pressure sensitive insoles (Fig. 4), both calibrated with the same method but manufactured with different electrical circuitry design (through mode in sensor 14 and shunt mode in sensor 15) the viscosities ranged from 13.37% to 16.92% (14.69 ± 0.69%), and from 1.58% to 12.05% (7.28 ± 2.94%), respectively. Even worse, there was a significant difference between the average viscosities of the 3 different layers of sensor structure 15 (Fig. 5): in layer A, $100\eta = 10.27 \pm 1.07\%$; in layer B, $100\eta = 7.08 \pm 1.94\%$; and in layer C, $100\eta = 4.49 \pm 2.06\%$. The viscosity of all 3 layers was significantly different (Kruskal-Wallis test: $p = 3.83E\text{-}13$; post hoc tests: Conover tests $p < 8E\text{-}07$; Dunn tests $p < 0.0017$).

Interestingly, comparing the viscosity of sensor structure 14 (through mode) to 15 (shunt mode), the average viscosities were 14.69% and 7.28%, respectively, which means that the shunt-mode-compatible piezo-resistive ink was less viscous than the through-mode-compatible ink, by an average η-differential of 7.41% (Fig. 5). Both sensor arrays were calibrated with the same device (Trublu).

4. Discussion

The method suggested in this paper is a dynamic one. As already explained in the introduction, static testing (relaxation and creep) takes a long time for obtaining accurate results. The reason for this is that a sensor cannot be loaded instantaneously with a material testing machine, i.e. by means of a Heaviside function of the displacement, so that a ramp function is required. The latter results in an overshoot of the load, which only gradually and asymptotically approaches the expected (i.e. true) stress relaxation rate (Fuss, 2012). Therefore, static testing tends to overestimate the viscosity, if insufficient time is allocated for experiments. Viscosity is also strain dependent (Fuss, 2012), and therefore also load dependent, as stress is a function of strain. This phenomenon was seen by the authors in Vinyl sensors under high pre-compression (unpublished results) when the conductivity decreased very slowly under fast unloading. The same effect becomes evident if the signal correction for determining the magnitude of η results in a figure-of-8 curve, i.e. undercorrection at high loads and overcorrection at low loads (yet the sum of the areas under the curve still equals 0).

The 'electrical viscosity' is usually, but not always, dependent on the solid viscosity (i.e. the mechanical properties of the sensor material). Foams, used for electrostatic materials with a piezoresistive side effect, exhibit large η (Table 1), which partially is caused by buckling (of cell edges) and pneumatic spring effects (Fuss, 2015b). The electrical viscosity is worsened if an additional viscous material is used in series with the sensor. This material can be a spacer for the purpose of loading (and calibrating) a specific sensor out of a sensor array; or foam padding e.g. in a scoliosis brace, if the sensor is intended to measure the pressure between skin and brace. This principle was demonstrated in the current research, namely that the same sensor exhibits different viscosity values when loaded by a stiff (wooden) and two different soft (silicone rubber, and unspecified rubber) spacers (Table 1, sensor structure no. 11, 12 and 13). The specific viscosities obtained were 4.8%, 11% and 16.9% for wooden spacer, silicone rubber spacer, and unspecified rubber sheet (trublue), respectively, where 16.9% is the 2nd worst viscosity shown in Table 1. This result seriously questions the accuracy of the trublue calibration device (Novel, Germany), even if the Pedar insole calibrated with trublue comprises of capacitative sensors and not of piezoresitive sensors. Any dynamic loading of a viscous material placed on top of a sensor increases the viscosity of the sensor.

Although Pang et al. (2012) suggest that electrical '*hysteresis may be attributed to … viscoelastic effects of the PDMS … layers*' (*PDMS* = Polydimethylsiloxane [silicon-based organic polymer]), it has never been described before that the viscous material of the air bladder, used in devices for testing and calibration of pressure sensors, can make such a big difference in electrical viscosity, and therefore also in accuracy, of one and the same sensor, tested with and without the bladder material. These differences in sensor viscosity within a sensor array could,

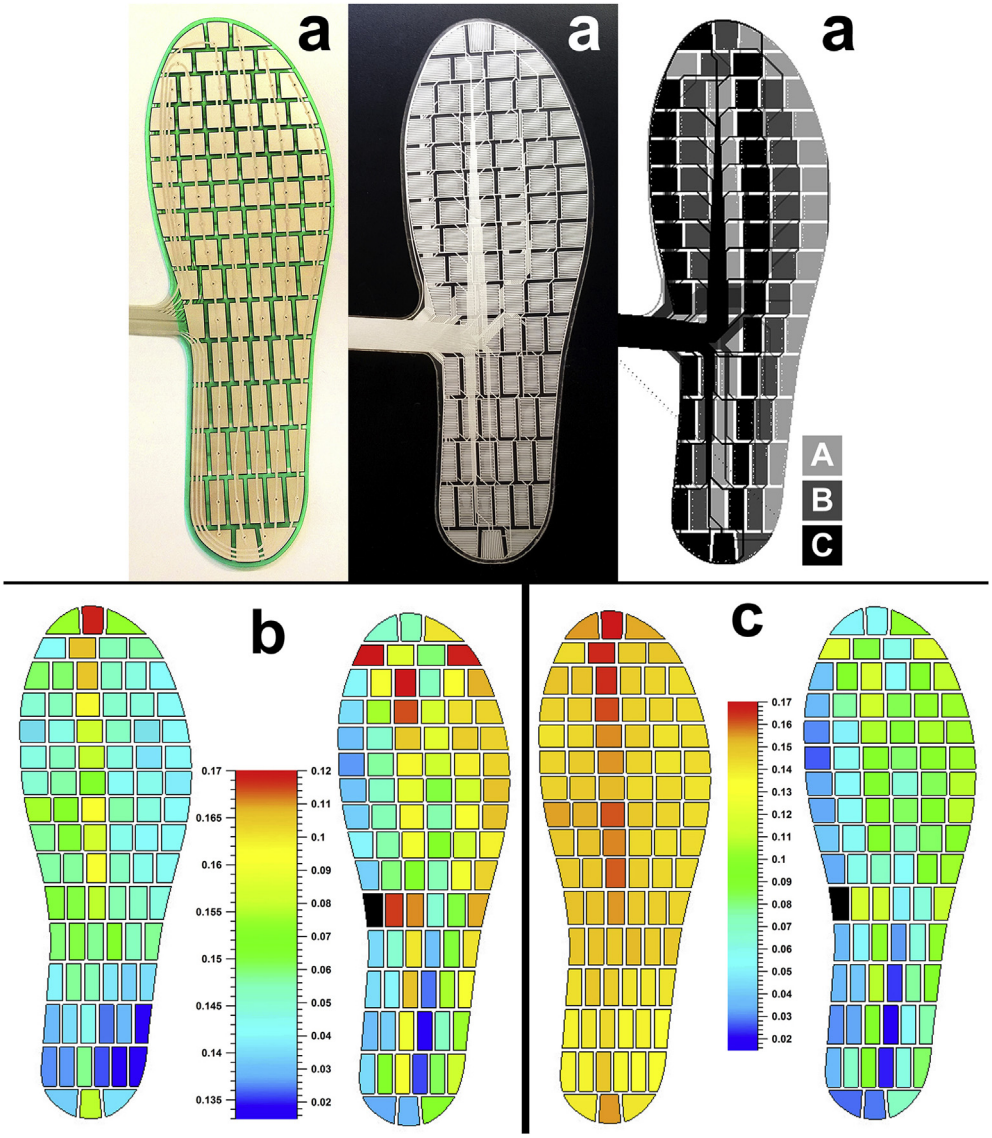

Fig. 4. a: printed pressure sensor arrays (insoles 1 and 2, through and shunt mode, respectively; cf. Table 1), and layer design of insole 2 (A, B, C = layer code); **b**: viscosity data colour coded (the colour scale corresponds to the range of minimum to maximum viscosity data of *each single* insole; **c**: viscosity data colour coded (the colour scale corresponds to the range of minimum to maximum viscosity data of *both* insoles. (For interpretation of the references to colour in this figure legend, the reader is referred to the Web version of this article.)

theoretically, depend on inconsistent properties of the air bladder material. However, as shown in the layered pressure sensitive insole (sensor 15, Table 1), there is even a significant difference in the averages of sensor viscosity between the different layers, which rules out any influence of hypothetical inconsistent properties of the air bladder material.

The effect of a visco-elastic material, in series with a sensor, on the calibration of this sensor depends on the calibration method. The methods for choice are dynamic and static ones. The dynamic method is characterised by a force or pressure gradient, exemplified by cyclic testing (sinusoidal or [linear/non-linear] triangular; the latter test was used in this study for all sensors listed in Table 1). The static testing involves incrementally increasing loads that are kept constant for a certain amount of time (step function). In the dynamic test, any additional viscous material placed on the sensor compromises (i.e. worsens) the sensor's viscosity (as shown in Table 1). In the static test, any additional viscous material placed on the sensor creeps as does the sensor, but does not cause the sensor to creep faster. This seems to be of advantage, however, the sensor's creep alone is already a disadvantage and compromises the calibration process. Either way, both calibration methods, be they dynamic or static, have their disadvantages.

Examples of pressurised devices mentioned above are the Trublu calibration device and a comparable experimental device ('custom pneumatic bladder pressure tester') with an unspecified membrane (Giacomozzi, 2010). The Trublu device recommends the (quasi)static method for calibrating Pedar insoles (Novel GmBH Inc, Munich, Germany); however, we used Trublu with the dynamic method (one loading/unloading measurement cycle). Giacomozzi (2010) also used her experimental device dynamically '*to deliver pressure ramps of loading*' to the sensors tested.

If, however, a piezo-electric sensor is calibrated with step-wise increasing loads (quasistatically) while the sensor is placed on a soft material (Pamar et al., 2017), then the material's viscosity does not compromise (i.e. worsen) the sensor's viscosity. The reason for this is that the soft viscous material certainly is subjected to creep (reduction of thickness), however the stress of the material does not change since the load is kept constant. This principle also applies to quasistatic Trublu calibration. Any quasistatic method, however, results in signal

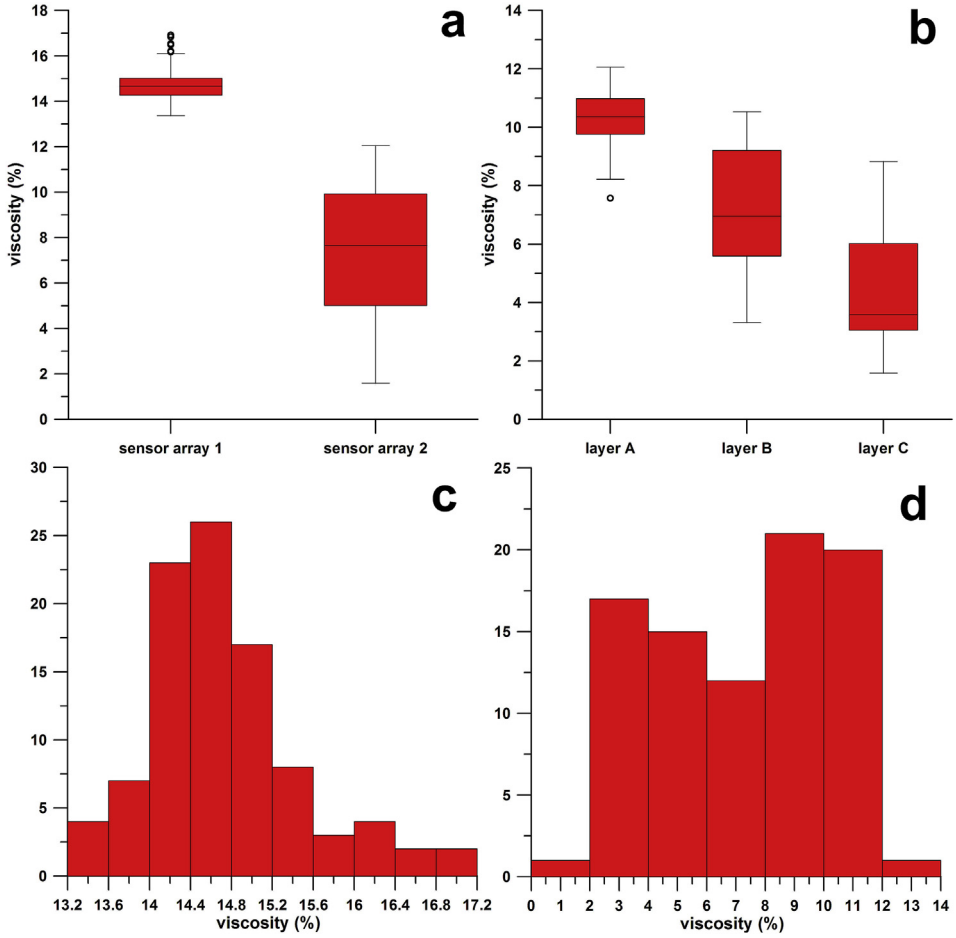

Fig. 5. a: box plot of the viscosities of the 2 printed pressure sensor arrays (insoles 1 and 2, through and shunt mode, respectively), ○ = outliers; **b**: box plot of the viscosities of the 3 layers (A, B, C; cf. Fig. 4a) of the 2nd printed pressure sensor array (insole 2, shunt mode); histogram of the viscosities of the printed pressure sensor arrays 1 (**c**) and 2 (**d**).

creep, i.e. non-linear increase of the signal (i.e. conductivity) over time.

Quantitative measurement methods for assessment of viscosity that have been used in the past include:

- Cyclic (sinusoidal) tests and determination of the "*%hysteresis*" (Giacomozzi, 2010). Comment: it is unclear why the hysteresis was assessed if the loss tangent could have been determined from the phase shift of the cyclic test data. (Annotation: hysteresis% is 100 times the ratio of Δy to range(y) of the data on the y-axis, with the y-data taken at the midpoint of the hysteresis on the x-axis, where the midpoint is the average of x_{min} and x_{max}).
- Creep by calculating the pressure (p) gradient ($\Delta p/\Delta t$) over 40 s of the loading period (Giacomozzi, 2010). Comment: it would have been better to determine the gradient from $dp/d(\log t)$ or $d(\log p)/d(\log t)$ at large t, depending on whether the creep function follows log- or power laws, respectively. Based on the creep function, piezoresistive sensors were found to follow a power law rather than a log law (Weizman and Fuss, 2015; Weizman, 2016).
- Creep (misnamed as 'drift'), by calculating the change in voltage over a defined time period, expressed as a percentage change relative to the initial voltage Vi, i.e. 100 $\Delta V/Vi$ (Pamar et al., 2017).

As there is no consensus on piezoresitive sensor characterisation available, an industry standard is overdue. This standard is preferably two-fold, and extend to the properties of piezoresistive inks as well as to the printing process. As inks produced only by a few companies (e.g. Creative Materials Incorporated, Massachusetts, United States) and no properly published research in viscosity is available (be it characterisation or reduction), the viscosity value must be shown in addition to the usual "resistance vs force curve". Yet even the latter requires more in-depth characterisation, as usually only a single curve (i.e. in-hysteretic, thereby suggesting that the ink is inviscid) is provided, thus suggesting that the sensor is inviscid. Sensitronics (2018) for example, claim that some of their sensors are 'low drift' but no supporting values are provided, other than the ones shown in Table 1. These values would exhibit good practice awareness, and would be invaluable to the customer, for selecting the best-performing ink for their purposes and products.

As far as the quality control of the printing process is required, companies specialised in printing piezoresistive sensors are encouraged to use a standardised calibration process (being aware that air-bladder methods with viscous rubber sheets or bladders introduce further sensor viscosity) and provide a map by indicating the resistance or (preferably) the conductance of the unloaded sensor as well as the viscosity values, comparable to the colour-coded maps shown in Fig. 4. These data as well as their visualisation can be generated quickly from the raw data of the calibration process in Matlab. Statistical processing of these results, (e.g. standard deviation and range of viscosity values) would account for the printing quality. The printing process can be compromised by the method (e.g. screen printing provides a more consistent sensor layer thickness than ink jet printing; Midori/Woo, 2016, personal communication), as well as by the mixing process of the piezoresitive ink. Therefore, the varying concentration of conductive particles during the course of the printing process (expressed in

conductance inconsistencies), due to sedimentation, can also affect the viscosity. More matrix material and therefore less carbon particles would correspond to more viscosity and less conductivity.

The method provided in this paper is not only applicable to determine the sensor viscosity, but also to signal correction of data collected from wearable devices. It has to be borne in mind, though, that the method is mathematically demanding for long-term real-time measurements (e.g. in wearable devices, worn and measured over hours at higher sampling rates, such as walking). The overall equation, i.e. Eq. (17), that is solved for this purpose at $t = n$ is a sum of $fn+1$ individual equations, which become more, and thus have to be updated, every dt ($= 1/f$) time step (where f is the data sampling frequency). Conversly, the advantage is that the error arising from hysteresis is reduced to almost zero, as there is only one single calibration function based on almost equal loading and unloading conductivities after correcting the signal (Fig. 3).

The method provided in this paper is also suitable for characterising the viscosity of power-law visco-elastic solids ('springpots'; Scott Blair, 1947), by calculating the strain's fractional derivative, whose fractional order corresponds to the viscosity constant η.

5. Proposal for industry standard

1) The piezoelectric sensor, whose viscosity is determined through this proposed standard, is subjected to standardized dynamic loading/unloading, up to the required peak force (corresponding to peak pressure of peak force over sensor area);
2) 10 conditioning or set cycles (transient phase) plus 5 measurement cycles are applied to the sensor;
3) The viscosity is determined for the last 5 cycles as per method suggested in this paper, by finding the fractional time derivative of the conductance, whose fractional order reduces the pressure - conductance hysteresis to zero and thus corresponds to the sensor's viscosity;
4) The sensor properties are reported as average, standard deviation and range of the viscosities of the 5 cycles; for sensor arrays also the average viscosity, standard deviation and range of all individual cell viscosities are reported;
5) The average absolute force rate (e.g. N/s) is reported [note that the deflection rate or strain rate is of little use as it depends on the stiffness of the spacer or sensor substrate material; the stiffer, the smaller the deflection rate at the same force rate];
6) The material of any spacer used for loading has to be reported, or the material of any rubber bladder or sheet, including their viscosities (to be determined with the same method suggested in this paper; from the stress – strain curve).
7) This standardized method also provides the calibration curve of each single sensor, which can be reported as an add-on value for the customers.

6. Conclusions

Electrical viscosity causes hysteresis, which compromises the calibration process and thus the accuracy of a sensor. The suggested method for collapsing the hysteresis by means of calculating the fractional time derivative of the conductance is suitable for fast and accurate determination of the electrical viscosity of a pressure sensor. The viscosity varies greatly across different pressure sensors and even within a single pressure sensor array. This variation reflects the quality of manufacturing. An industry standard is required that informs the customers of the viscosity's magnitude, such that the customers are able to select the sensors with the least viscosity for improving the accuracy of their products.

CRediT authorship contribution statement

Franz Konstantin Fuss: Formal analysis, Writing - original draft, Writing - review & editing. **Adin Ming Tan:** Formal analysis, Writing - original draft, Writing - review & editing. **Yehuda Weizman:** Formal analysis, Writing - original draft, Writing - review & editing.

References

Abel, N.H., 1823. Oplösning af et par opgaver ved hjelp af bestemte integraler [*Solution of some problems with the help of definite integrals*]. Magazin Naturvidenskab 1 (2) (Christiania, Norway).

Ding, T., Wang, L., Wang, P., 2007. Changes in electrical resistance of carbon-black-filled silicone rubber composite during compression. J. Polym. Sci. B Polym. Phys. 45, 2700–2706.

Fuss, F.K., 2012. Nonlinear visco-elastic materials: stress relaxation and strain rate dependency. In: Dai, L., Jazar, R.N. (Eds.), Nonlinear Approaches in Engineering Applications. Springer, New York, pp. 135–170.

Fuss, F.K., 2015a. The loss tangent of visco-elastic models. In: Dai, L., Jazar, R.N. (Eds.), Nonlinear Approaches in Engineering Applications: Applied Mechanics, Vibration Control and Numerical Analysis. Springer, New York, pp. 137–157.

Fuss, F.K., 2015b. The design strain and dead mass of energy absorbing materials and structures: mathematical principles and experimental determination. Process Eng. 112, 116–121.

Giacomozzi, C., 2010. Appropriateness of plantar pressure measurement devices: a comparative technical assessment. Gait Posture 32, 141–144.

Giovanelli, D., Farella, E., 2016. Force Sensing Resistor, evaluation of technology for wearable body pressure sensing. J. Sensors 2016https://doi.org/10.1155/2016/9391850. 9391850.

Gong, S., Lai, D.T.H., Su, B., Si, K.J., Ma, Z., Yap, L.W., Guo, P., Cheng, W., 2015. Highly stretchy black gold E-skin nanopatches as highly sensitive wearable biomedical sensors. Adv. Electron. Mater. 1 (4), 1400063. https://doi.org/10.1002/aelm.201400063.

Hall, R.S., Desmoulin, G.T., Milner, T.E., 2008. A technique for conditioning and calibrating force-sensing resistors for repeatable and reliable measurement of compressive force. J. Biomech. 41, 3492–3495.

Kalantari, M., Dargahi, J., Kövecses, J., Mardasi, M.G., Nouri, S., 2012. A new approach for modeling piezoresistive force sensors based on semiconductive polymer composites. IEEE ASME Trans. Mechatron. 17 (3), 572–581.

Kost, J., Foux, A., Narkis, M., 1994. Quantitative model relating electrical resistance, strain, and time for carbon black loaded silicone rubber. Polym. Eng. Sci. 34 (21), 1628–1634.

Lacasse, M.-A., Duchaine, V., Gosselin, C., 2010. Characterization of the electrical resistance of carbon-black-filled silicone: application to a flexible and stretchable robot skin. In: IEEE International Conference on Robotics and Automation (ICRA), May 2010, pp. 4842–4848.

Lu, Y., Biswas, M.C., Guo, Z., Jeon, J.-W., Wujcik, E.K., 2019. Recent developments in bio-monitoring via advanced polymer nanocomposite-based wearable strain sensors. Biosens. Bioelectron. 123, 167–177. https://doi.org/10.1016/j.bios.2018.08.037.

Oldham, K.B., Spanier, J., 1974. The Fractional Calculus. Academic Press Inc, New York.

Oppermann, K., Arminger, B., Zagar, B., 2010. Smart hysteresis compensation of a magneto-elastic force sensor based on Terfenol-d. In: 2010 IEEE International Conference on the Instrumentation and Measurement Technology Conference (I2MTC), May 2010, pp. 662–667.

Pamar, S., Khodasevych, I., Troynikov, O., 2017. Evaluation of flexible force sensors for pressure monitoring in treatment of chronic venous disorders. Sensors 17, 1923. https://doi.org/10.3390/s17081923.

Pang, C., Lee, G.-Y., Kim, T., Kim, S.M., Kim, H.N., Ahn, S.-H., Suh, K.-Y., 2012. A flexible and highly sensitive strain-gauge sensor using reversible interlocking of nanofibers. Nat. Mater. 11, 795–801. https://doi.org/10.1038/NMAT3380.

Preisach, F., 1935. Über die magnetische Nachwirkung. Z. Phys. 94 (5–6), 277–302.

Scott Blair, G.W., 1947. The role of psychophysics in rheology. J. Colloid Sci. 2, 21–32.

Sensitronics, 2018. Sensitronics products. Available: https://www.sensitronics.com/products.php, Accessed date: 2 August 2018.

Sircar, A.K., Voet, A., Cook, F.R., 1971. Relaxation of stress and electrical resistivity in carbon-filled vulcanizates at moderate and high extensions. Rubber Chem. Technol. 44 (1), 185–198.

Sun, H.G., Zhang, Y., Baleanu, D., Chen, W., Chen, YangQuan, 2018. A new collection of real world applications of fractional calculus in science and engineering. Commun. Nonlinear Sci. Numer. Simul. 64, 213–231. https://doi.org/10.1016/j.cnsns.2018.04.019.

Voet, A., Cook, F.R., Sircar, A.K., 1971. Relaxation of stress and electrical resistivity in carbon-filled vulcanizates at minute shear strains. Rubber Chem. Technol. 44 (1), 175–184.

Wang, L., Ding, T., Wang, P., 2009. Research on stress and electrical resistance of skin-sensing silicone rubber/carbon black nanocomposite during decompressive stress relaxation. Smart Mater. Struct. 18, 065002. https://doi.org/10.1088/0964-1726/18/6/065002.

Wang, L., Ma, F., Shi, Q., Liu, H., Wang, X., 2011. Study on compressive resistance creep and recovery of flexible pressure sensitive material based on carbon black filled silicone rubber composite. Sensor. Actuator. 165, 207–215.

Weizman, Y., 2016. Smart Football Footwear for Advanced Performance Analysis and Training Purposes. PhD (Mech Eng) thesis. RMIT University, Melbourne, Australia.

Weizman, Y., Fuss, F.K., 2015. Viscosity of Piezoresistive Materials. Internal Report. RMIT University, Melbourne, Australia.

Weyl, H., 1917. Bemerkungen zum Begriff des Differentialquotienten gebrochener Ordnung. Vierteljahrsschrift der Naturforschenden Gesellschaft Zürich 62, 296–302.

Zheng, Q., Zhou, J.F., Song, Y.H., 2004. Time-dependent uniaxial piezoresistive behavior of high-density polyethylene/short carbon fiber conductive composites. J. Mater. Res. 19, 2625–2634.